Contents lists available at ScienceDirect

Fusion Engineering and Design

journal homepage: www.elsevier.com

Characterization of the helicon plasma flux to the target of Proto-MPEX

C.J. Beers[a, *], E.G. Lindquist[a], T.M. Biewer[b], J.F. Caneses[b], J.B.O. Caughman[b], R.H. Goulding[b], N. Kafle[a], H. Ray[a], M.A. Showers[a], S.J. Zinkle[a, b], J. Rapp[b]

[a] University of Tennessee – Knoxville, Knoxville, TN, 37996, USA
[b] Oak Ridge National Laboratory, Oak Ridge, TN, 37831, USA

ARTICLE INFO

Keywords:
Proto-MPEX
Ion flux
Helicon antenna

ABSTRACT

The ITER divertor will have to handle the boundary plasma power exhaust in the form of high heat and particle flux. The Prototype Material Plasma Exposure eXperiment (Proto-MPEX) is a plasma source development device for the proposed Material Plasma Exposure eXperiment (MPEX), which is intended to create fusion reactor divertor-like plasma conditions for studying plasma material interactions. Here, ion fluxes to various targets within Proto-MPEX are found to be $5 \pm 2.5 \times 10^{23}\,m^{-2}s^{-1}$ when using only a helicon plasma source. The fluxes along the flux tube are compared for both 30 cm in front of the target and a few cm in front of the target. The emission intensity fall-off distance in front of the target is studied via Balmer series from a visible camera looking at the target. This fall-off distance of ~2–4 cm and the dissociation and ionization mean free path of D_2 being over 0.5 m leads to a conclusion that Proto-MPEX is not in a high recycling regime with helicon only plasmas.

1. Introduction

In a tokamak such as ITER, the divertor is designed to handle the heat and particle fluxes exhausted by the edge plasma, where open field lines will terminate. In ITER, the heat flux perpendicular to the divertor face will be up to 10 MW/m^2 for steady-state [1]. Electron temperatures along with ion temperatures in the divertor are expected to be in the range of 1–15 eV and ion fluxes of up to $10^{24}\,m^{-2}s^{-1}$ are expected at the divertor surfaces [2]. These challenging ITER-like divertor conditions produce numerous plasma material interactions (PMI) in the divertor that need further study to understand and predict the divertor behavior.

Linear devices allow for easier PMI studies than a tokamak due to their availability for dedicated PMI studies and easy access of diagnostics. Several linear devices have been constructed to study PMI but cannot fully reach the conditions of the divertor [3,4]. The planned Material Plasma Exposure eXperiment (MPEX) is designed to meet these ITER and future fusion reactor divertor-like conditions [5]. The Prototype-Material Plasma Exposure eXperiment device (Proto-MPEX) is a plasma source R & D device for MPEX and has already met many of the desired plasma conditions [6,7].

Steps are now being taken for Proto-MPEX to meet the desired target conditions (ion flux, ion temperature, and heat flux). The ion temperature measurements have been described elsewhere [8] as well as the heat flux measurements [9,10]. The desired target conditions for MPEX can only be reached via high recycling and to access this regime there needs to be a conduction-limited parallel transport regime [11]. This regime involves high recycling to reach an increased flux to the target but for lower input powers the transition from high recycling to a recombining plasma can pose to be a problem. At temperatures below ~5 eV, plasma flux rollover can occur which involves a loss of parallel plasma momentum because of charge exchange with neutrals [12]. If temperatures reach below ~1 eV the plasma can detach due to volumetric recombination which prevents any flux from getting to the material's surface.

The high recycling regime has been explored on Proto-MPEX previously when a Trivelpiece-Gould (T-G) edge peaked heating mode was used [13] but Proto-MPEX has since achieved a core peaked heating

* Corresponding author at: Oak Ridge National Laboratory, 1 Bethel Valley Road, Oak Ridge, TN, 37831, USA.
Email address: beerscj@ornl.gov (C.J. Beers)

https://doi.org/10.1016/j.fusengdes.2018.11.056
Received 6 September 2018; Received in revised form 27 November 2018; Accepted 30 November 2018
Available online xxx
0920-3796/

scheme [14,15]. This paper characterizes the incident ion flux and the role of recycling on that flux for various targets in Proto-MPEX using a core peaked plasma density from a helicon only source plasma.

2. Experimental

2.1. Proto-MPEX setup

Proto-MPEX utilizes a helicon antenna as its primary plasma source, which is discussed elsewhere both about its physical design [6] and modes of operation [16]. Deuterium was used as the primary working gas for all experiments but not kept constant for each target. The magnetic field and geometry of Proto-MPEX used for the experiments is shown in Fig. 1. The helicon input power was 90 kW and no auxiliary heating (electron or ion cyclotron heating) was on during spectroscopic measurements or plasma density and temperature measurements.

Proto-MPEX uses a suite of diagnostics to measure plasma parameters (plasma electron density and temperature) on a plasma discharge (shot) to shot basis, many of which are discussed by Caughman et al. [6]. Here, only diagnostics utilized will be discussed in further detail.

A double Langmuir probe (DLP) is installed 2.3 m from the helicon antenna and 30 cm in front of the Thomson scattering location, as shown in Fig. 1, to measure the plasma density and temperature far away from the target. A skimmer separates the DLP and target regions making the DLP measurement not dependent on any target interactions The DLP design is chosen for its RF compensation as described by Caneses and Blackwell [17]. The DLP has molybdenum probe tips that are 1.8 mm in length, are 0.25 mm in diameter, and are separated by 1.4 mm. The probe dimensions are determined by placing a ruler next to the tips, taking a picture, and counting pixels for size determination. A ceramic sleeve holds the Mo probe tips in place. The area of the tips used is the whole surface area of the exposed probe tips because it gives a more conservative value for the plasma density. The plasma temperature and density are determined following the analysis outlined in Beal et al. [18].

To also measure the plasma density and temperature close to the target, a Thomson scattering laser system is used as described by Biewer et al. [19]. The Thomson scattering system is fixed in location in front of the target, and plasma density and temperature reported here are during the flat top region of the high-density helicon mode of operation.

An Edgertronic SC1 camera looks through a window and gate valve to view the target. The camera framerate is 1 kHz with pixel dimensions of 688 × 864. The size of the pixels is calculated by using a known bolt size in a camera image and counting pixels. The camera is used with narrowband filters that allow for viewing ~10 nm of visible light. The filters used are for the deuterium series Balmer emission lines for the $n = 3$ to $n = 2$ (D_α), $n = 4$ to $n = 2$ (D_β), and $n = 5$ to $n = 2$ (D_γ). The cameras are absolutely calibrated using a calibrated white light integrating sphere, the shutter speed for controlling the integration time, and the known filter transmissions curves. Each filtered image taken includes a different shutter speed that is calibrated out to have comparable data.

2.2. Proto-MPEX's June 2017-May 2018 campaign target study

A 0.25″ thick ATJ graphite disk from Union Carbide (now GrafTech) was used as the target from June 2017-Jan. 2018. An embedded ion flux probe and a set of four DLPs were installed in the target which are referred to as the target ion flux probe and target DLPs, respectively. This target was constructed to measure the plasma properties and ion flux directly at the target. The sample surface was in the as-received (no sample cutting, surface polishing, or heat treatment) state for exposure. The probes consisted of alumina ceramic around molybdenum collecting wires. Fig. 2 shows the target a) front face with each of the five probes being 1.43 cm apart and the center one being the single wire ion flux probe and b) the location of the Thomson scattering laser in air at ~4 cm in front of the target. The probe tips were ground flush with the graphite surface to reduce any sheath effects and to make the flux calculation simpler due to no probe tip length being present (probe area is cross sectional area of the wire). The ion flux collecting wire was 1 mm in diameter while the DLPs had 0.75 mm diameter wire. An ion flux was calculated using the plasma density and temperature assuming Bohm conditions to compare to the saturation current collected by the flux probe via: [20]

$$\begin{aligned}\Gamma_{se} &= 0.61 * n_{se} * c_s \\ &= 0.61 * n_{se} * \sqrt{k_B \left(\frac{T_e + \gamma * T_i}{m_i} \right)} \\ &= e * j_{sat}(s), \left[ions\ m^{-2}\ s^{-1} \right]\end{aligned} \tag{1}$$

where Γ_{se} [ions m^{-2} s^{-1}] is the ion flux to the sheath entrance, n_{se} [m^{-3}]

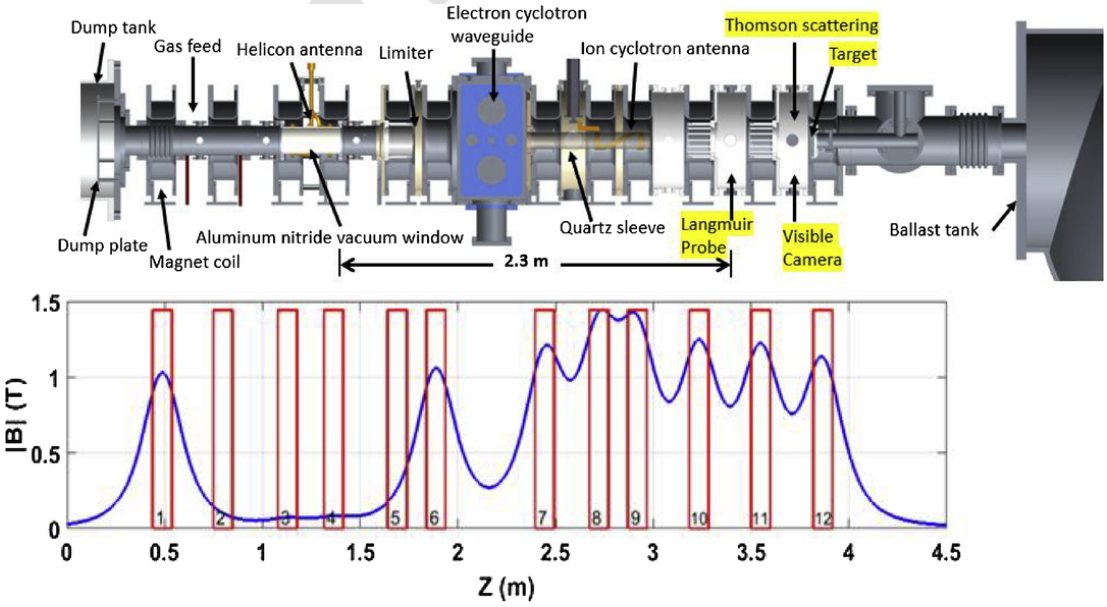

Fig. 1. Proto-MPEX cross-section showing location of diagnostics used in highlight and the magnetic field used for all experiments. The magnetic field profile is in blue and the red boxes, numbered 1 through 12, are the magnets. (For interpretation of the references to colour in this figure legend, the reader is referred to the web version of this article).

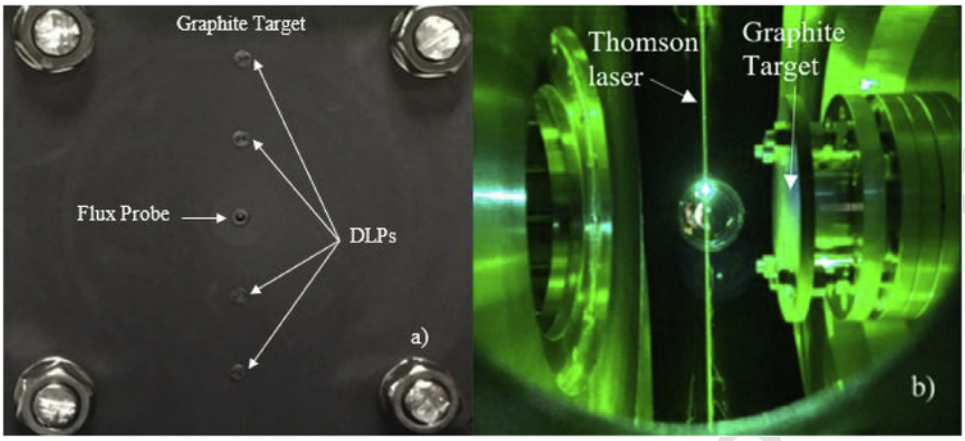

Fig. 2. Graphite target views of a) embedded double Langmuir probe array and center ion flux collecting probe and b) target view from visible camera port showing Thomson scattering laser in air with distance of ~4 cm in front of the target.

is the density at the sheath entrance or plasma density, c_s [m s^{-1}] is the sound speed of ions, k_B is the Boltzmann constant, T_e [eV] is the plasma electron temperature, γ is 3 for adiabatic flow, T_i [eV] is the plasma ion temperature, which was assumed to be equal to T_e, m_i [g] is the mass of the plasma ions, e is the elementary charge, and j_{sat} [ions m^{-2} s^{-1}] is the ion saturation current incident on the probe area.

A stainless-steel target was installed from Jan. 2018-April 2018. The target was on a movable bellows system as shown in Fig. 3 in order to measure the plasma density and temperature from Thomson scattering closer to the target. The scan distance enabled by the bellows ranged from 8 cm behind the target to directly in the path of the Thomson system. The target was a water blasted 0.25 mm thick piece of 304 stainless-steel. The water blasted surface enhanced the IR imaging.

A 3 mm thick chemical vapor deposition (CVD) silicon carbide (SiC) (SC-003 variant) target produced by PermaTech was used during the April 2018- May 2018 campaign. The SiC has chemical purity of greater than 99.9995%. The sample surface was in the as-received state for exposure. The SiC disk was housed inside a 310-stainless-steel holder. An image of the front face of the SiC assembly is shown in Fig. 4. The target assembly was mounted again on the moveable bellows system but only used at the closest location to the target that the Thomson scattering could collect data.

3. Results and discussion

3.1. Machine conditions

The same operating magnetic field for all experiments was used as shown in Fig. 1. The input helicon power is given in Fig. 5 along with the time chosen to take the spectroscopic traces as the dashed line. The input power was similar, but slightly less for the SiC target, for the time traces taken along with the magnetic field being the same for all plasma discharges. No pressure gauge was available near the target to observe pressure change through the length of the pulse.

3.2. Ion flux

The plasma density and temperature were measured using the DLP 30 cm in front of the target and Thomson scattering at 4 cm in front of the graphite target, 1.5, 1.75, 2, and 4 cm in front of the stainless-steel target, and 2.75 cm in front of the SiC target. The DLP and Thomson scattering are both collecting data at the center axis of the machine. The graphite target also used the above center target DLP to get plasma density and temperature at the target. The plasma core is 3 cm in diameter and the target DLP is 1.47 cm above the center, so it is still representative of the location of the DLP, Thomson, and flux probe. Proto-MPEX has flat electron temperature profiles across the plasma radius and has a plateaued electron density in the core [7]. The closest Thomson locations used here are the closest that the target could get to the laser before the stray-light peak would overtake the Thomson signal.

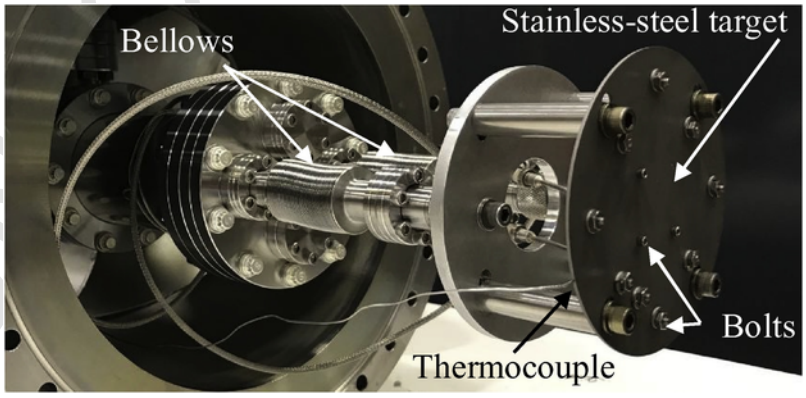

Fig. 3. Stainless-steel target attached to bellows to allow for target movement with respect to the Thomson scattering location. A thermocouple was inserted in the side of the target to compare to IR imaging. Bolts of same type in target face hold a target heater not used in these experiments.

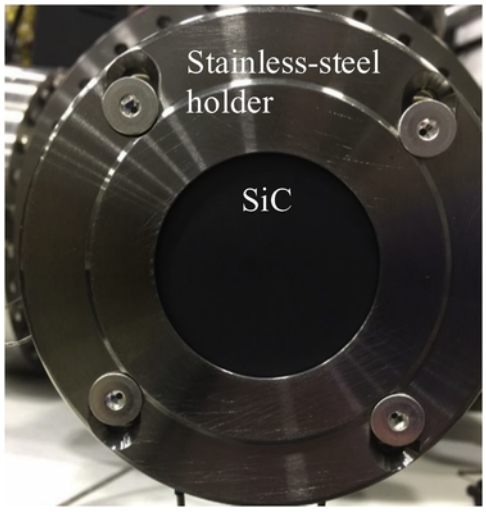

Fig. 4. The face of the SiC target assembly on a moveable bellows system with front plate.

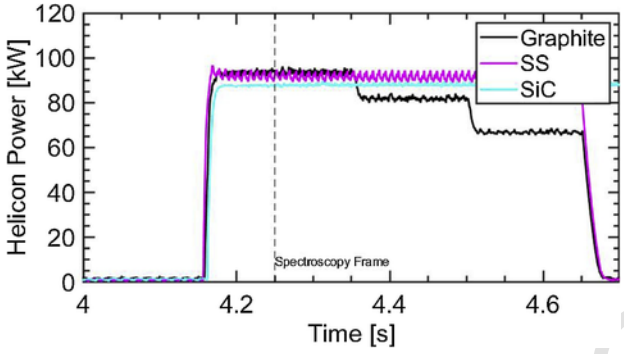

Fig. 5. The helicon input power and time used for the spectroscopic frame for the three targets.

Fig. 6 shows the density and temperature for the various targets with their respective methods of collecting them. The amount of injected gas can vary between the targets in order to achieve a centrally peaked profile which leads to varying densities between the targets as measured by the DLP. The density and temperature both show a decrease near the target from the Thomson as compared to the upstream DLP except for the graphite target, which has the parameters the same at 4 cm from the target. The embedded probes do however so a decrease indicating the plasma parameter change must occur within 4 cm from the target. The stainless-steel target with multiple Thomson scattering points in front of the target also shows a decrease in parameters compared to the DLP 30 cm from the target. The dip in the measured Thomson on the stainless-steel target is not well understood and looking at the light emissions in front of the target to get a qualitative comparison is done in Section 3.3.to see if it is a real phenomenon. The SiC because of the less gas injected than that of the stainless-steel or graphite has a reduced density in front of the target. Silicon in the SiC also getters oxygen, which takes hydrogen with it, well which lowers the density further [21–23]. The width of the area in front of the target in which the plasma parameters change is similar to modelling done on Proto-MPEX done for T-G mode helicon plasmas [13] and for similar discharges involving electron cyclotron heating (ECH) [7]. B2.5-Eirene modelling was done based on the DLP data 30 cm in front of the target which does show a higher electron temperature in front of the target than what is measured both close to and at the target in this experiment [7]. However, the temperature was higher in those experiments which changes the ionization mean free path of the recycled particles.

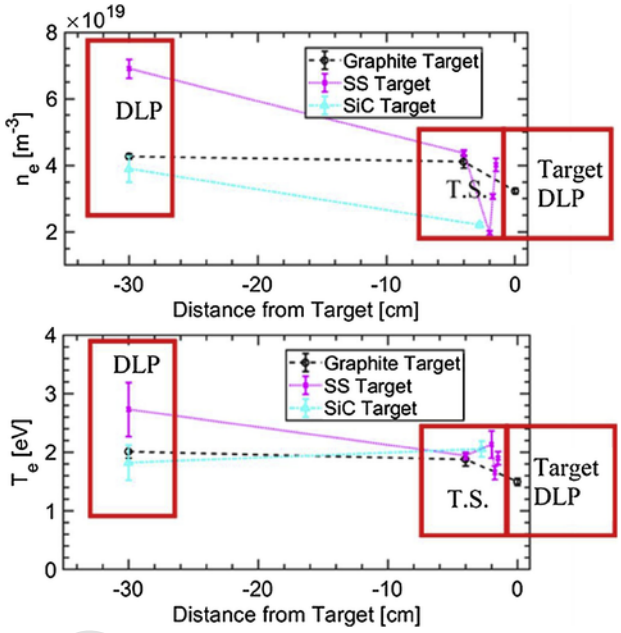

Fig. 6. Plasma density and temperature for the three targets from the DLP 30 cm in front of the target, the Thomson scattering system as close to the target as stray light would allow, and for the graphite target embedded DLP above the center ion flux probe. Red boxes hold the diagnostic and their respective data. The lines are to help guide the readers eye. (For interpretation of the references to colour in this figure legend, the reader is referred to the web version of this article).

Using the density and temperature from Fig. 6 and Eq. (1) the incoming ion flux value was calculated. Fig. 7 shows the calculated flux value and the directly measured flux from the graphite flux probe being $5 \pm 2.5 \times 10^{23}\,m^{-2}s^{-1}$. The large error bars come from the gap between the Mo collecting wire and the alumina ceramic around it. This gap can change the collection area leading to an overestimation; however, the calculated flux from plasma density and temperature from the target DLP is within the error bar. Thomson scattering in front of the target can be used as a good approximation of the flux to the target if the Thomson measurement is within the distance from the target in which the flux changes from that of the source. The exact size of this changing plasma parameter zone (fall-off width) will be discussed in Section 3.3.

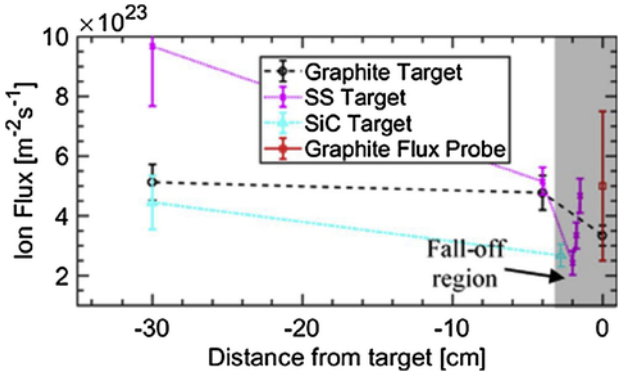

Fig. 7. Ion flux to the target calculated from the plasma density and temperature in Fig. 6 along with the directly measured ion flux to the graphite ion flux probe shown in red. A decrease in flux can be seen close (≤2.5 cm) to the target when compared to 30 cm away which is highlighted as the fall-off region. The lines are to help guide the readers eye (For interpretation of the references to colour in this figure legend, the reader is referred to the web version of this article).

3.3. Target recycling

To further investigate the change in ion flux in front of the target, the Balmer series line intensity emissions at the target is measured from visible cameras. A reference image on how the emissions were taken from the camera data is shown in Fig. 8. The Balmer series (D_α, D_β, and D_γ) intensity line traces for the three targets is shown in Fig. 9. The emission profile in Fig. 9 is also seen to decrease away from target. This feature will be referred to here as fall-off. The highest intensity is very near to the target face which is due to surface recombination. The D_α gives information about the ionization and the D_γ line is an indicator of three-body recombination (as temperatures are too low for ionization to be strongly dominating this is likely dominate). The line traces for the three targets D_γ emission is shown in Fig. 10 to look at the recombination front. The three targets show that the recombination starts to increase within 1–1.5 cm of the target face. The size of the recombination front can be compared to the dissociation and ionization mean free path of particles coming from the target to determine if a high recycling regime is present. The fall-off distance compared to the ionization mean free and dissociation of D_2 [24,25] is over 0.5 m for all plasma parameters observed, indicating that neutrals are leaving the plasma before being re-ionized. Single deuterium has an order of magnitude larger mean free path. The lack of flux increase due to recycling confirms this.

The D_β is compared to the behavior of the various modelled targets by Rapp et al. [7] where a carbon target has a higher intensity than one of iron. This matches the experimental results seen here. The carbon target also has a sharper fall-off in emissions than that of the iron as seen in the D_β profile. This is likely due to carbon's reduced reflected energy coefficient over iron which causes more particles to recombine at the target and increases observed emissions [26].

The flux fall-off is taken to follow the light emission fall-off profile in front of the target. The change in plasma parameters can also be mapped by the ratio of D_γ/D_α, as shown in Fig. 11. As the ratio rises the plasma parameters decrease [27,28]. These ratios show that the flux fall-off is within a cm or less, but each target has a different profile. The graphite target has plasma parameters decrease within 1 cm of the target face, the stainless-steel target plasma parameters decrease within 0.5 cm of the target, and the SiC has the largest plasma parameter decrease occurring within 1 cm of the target. The deviations in the stainless-steel occurring in the region of the Thomason scattering measurements match that of the drops and rises in the Thomson measurements but this phenomenon is not well understood at this time and needs further investigation. The fall-off distances are likely dependent on the upstream conditions where the higher density and temperature provide greater plasma pumping. This pumping effect moves neutrals that come off the target out of the plasma path and causes the recombination to be solely surface recombination. This likely isn't as strong for the SiC plasma which has lower electron temperatures that are in the range for molecular activated recombination and three-body recombi-

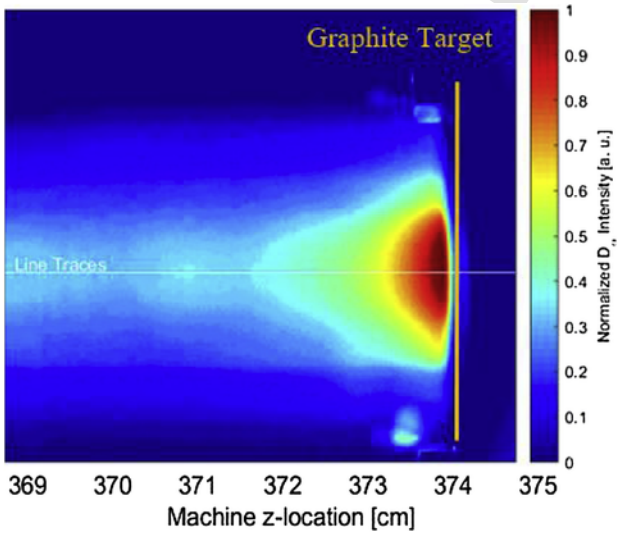

Fig. 8. Visible camera data for the frame at time = 200 ms into the pulse at 4 cm from the Thomson location. The graphite D_α is shown with a horizontal white trace that shows where the Balmer series is taken for plotting fall-offs. The orange vertical line shows the target location.

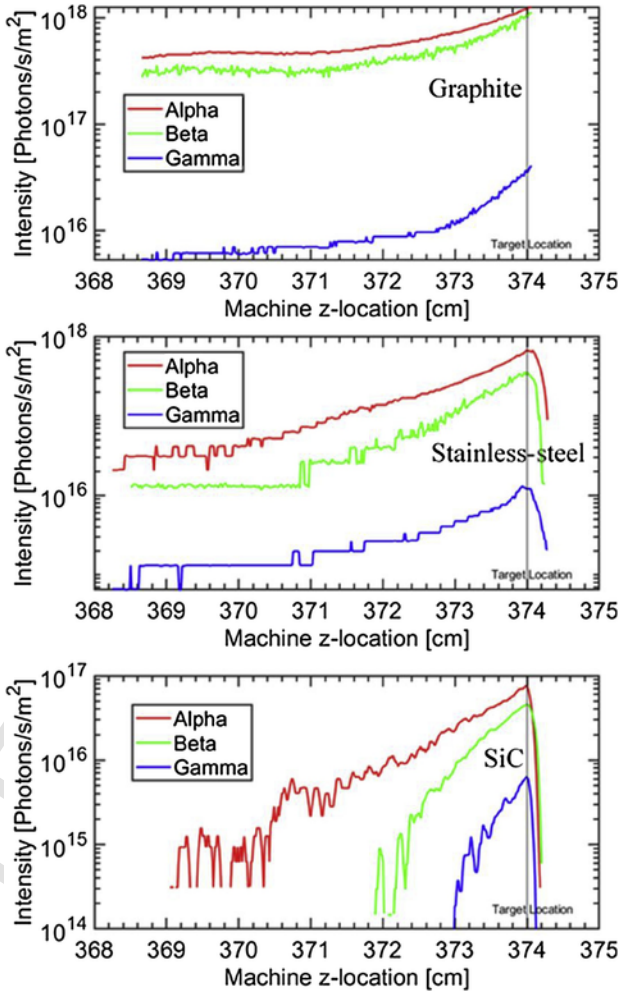

Fig. 9. The Balmer series D_α, D_β, and D_γ emissions along the line trace shown in Fig. 8 for the three targets. The fall-off widths of the targets are 2–4 cm.

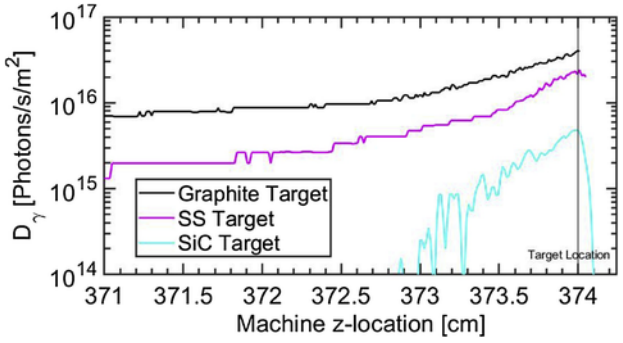

Fig. 10. Comparison of the D_γ emissions between the three targets indicating an increase in recombination in front of the targets.

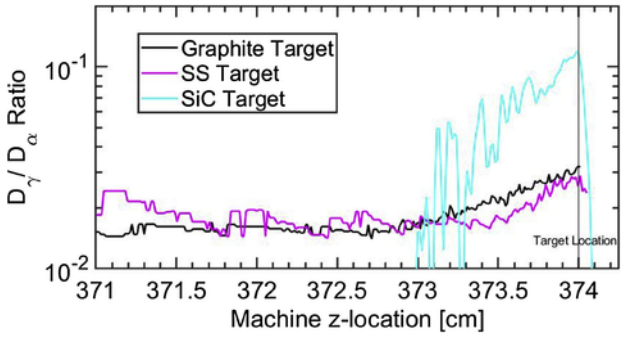

Fig. 11. Comparison of the Dγ/Dα ratios for the three targets as an indicator of the ionization front. The Dγ/Dα for the stainless-steel target can be seen to have the shortest distance in front of the target in which the ionization front disappears while the SiC shows the largest. See text for further details.

nation to play a role which could be causing higher losses both near and slightly farther away from the target rather than high recycling. The gettering effect of the Si can also lead to a reduced emission from less particles being present. Graphite shows a trend somewhere in the middle of stainless-steel and SiC where there the rise is similar to that of stainless-steel but occurs farther away from the target.

Proto-MPEX in the near future is putting a pressure gauge near the target to studies on the effect of the neutral gas pressure at the target and its role in delivered flux. The D_2 ionization and mean free path for ECH plasmas in Proto-MPEX have been measured as 2–3 cm which is on the same order for the Balmer emission fall-off distance [7] so plasma is not escaping the plasma column which is on the order of 5 cm and a high recycling regime is seen. The ECH experiment had similar densities to this experiment which indicates that higher ion temperatures are more important for Proto-MPEX to reach a high recycling regime. Metal targets will also need the least additional heating ($\geq$ 5 eV increase) to reach a conduction-limited regime. Proto-MPEX will need higher electron temperatures than the reported ~2 eV to reach a high recycling state and achieve the desired increased target flux. However, these fluxes are in the range of current PMI devices. These helicon-only ion flux values to the target show promise for the full MPEX device being able to reach desired fluxes of $\geq 1 \times 10^{24}\,m^{-2}s^{-1}$. Future work planned on Proto-MPEX will measure target flux at higher densities with ECH included.

4. Summary and conclusion

The ion flux has been measured close to the target for three materials: graphite, stainless steel, and SiC and compared to the source flux. An embedded ion flux collecting probe was also built to directly measure the flux at the surface. The ion flux measured was $5 \pm 2.5 \times 10^{23}\,m^{-2}s^{-1}$ and all other fluxes measured close to the target are within the error bars. The flux to the target was 50–60 % of the source ion flux measured ~30 cm in front of the target which. All fall-offs of flux were measured to be within 4 cm of the target. The recorded flux values are close (within a factor of 2) to MPEX's goal ion flux and excepted to reach the goal of $10^{24}\,m^{-2}s^{-1}$ via a high recycling regime with higher electron temperatures.

The recycling at the target was measured via visible cameras looking at the Balmer series (D_α, D_β, and D_γ) and the size of the Balmer series emission fall-off compared to that of the observed flux fall-off distance. The Balmer emission fall-off distance being 2–4 cm and the dissociation and ionization mean free path being much longer ($>$ 0.5 m) indicates that no high recycling regime is occurring as the particles leaving the target are lost. The Balmer D_γ/D_α ratio indicates that all targets go into high recombination $\leq$ 1 cm from the target as the density decreases and particles are lost. Stainless-steels and likely tungsten also will need the least additional heating to reach the high recycling regime due to their higher reflected energy coefficients which will help Proto-MPEX with low energy higher flux PMI studies.

Acknowledgements

The authors would like to thank the Proto-MPEX team for their support and aid in diagnostics and machine operation. This work was supported by the Oak Ridge National Laboratory managed by the UT-Battelle, LLC, for the U.S. Department of Energy under AE-AC05-00OR22725.

References

[1] R.A. Pitts, S. Carpentier, F. Escourbiac, T. Hirai, V. Komarov, A.S. Kukushkin, S. Lisgo, A. Loarte, M. Merola, R. Mitteau, A.R. Raffray, M. Shimada, P.C. Stangeby, Physics basis and design of the ITER plasma-facing components, J. Nucl. Mater. 415 (2011) S957–S964, https://doi.org/10.1016/j.jnucmat.2011.01.114.

[2] R. Behrisch, G. Federici, A. Kukushkin, D. Reiter, Material erosion at the vessel walls of future fusion devices, J. Nucl. Mater. 313–316 (2003) 388–392, https://doi.org/10.1016/S0022-3115(02)01580-5.

[3] B. Unterberg, R. Jaspers, R. Koch, V. Massaut, J. Rapp, D. Reiter, S. Kraus, A. Kreter, V. Philipps, H. Reimer, U. Samm, L. Scheibl, B. Schweer, J. Schuurmans, I. Uytdenhouwen, R. Al, M.A. van den Berg, S. Brons, H.J.N. van Eck, W.J. Goedheer, M.F. Graswinckel, T. van der Grift, A. Kleyn, W.R. Koppers, O. Kruyt, A. Lof, H.J. van der Meiden, W. Melissen, M. van de Pol, G.J. van Rooij, P. Smeets, J. Scholten, D.C. Schram, G. De Temmerman, W. Vijvers, P.A. Zeijlmans van Emmichoven, J.J. Zielinski, New linear plasma devices in the trilateral euregio cluster for an integrated approach to plasma surface interactions in fusion reactors, Fusion Eng. Des. 86 (2011) 1797–1800, https://doi.org/10.1016/j.fusengdes.2011.03.082.

[4] M. Sakamoto, K. Oki, Y. Nakashima, Y. Akabane, Y. Nagatsuka, M. Yoshikawa, R. Nohara, H.K. Hosoi, H. Takeda, K. Ichimura, J. Kohagura, M. Yoshikawa, M. Ichimura, T. Imai, Plasma, plasma characterization in divertor simulation experiments with a V-Shaped target on GAMMA10/PDX, Trans. Fusion Sci. Technol. 63 (2013) 188–192, https://doi.org/10.13182/FST13-A16902.

[5] J. Rapp, T.M. Biewer, T.S. Bigelow, J.B.O. Caughman, R.C. Duckworth, R.J. Ellis, D.R. Giuliano, R.H. Goulding, D.L. Hillis, R.H. Howard, T.L. Lessard, J.D. Lore, A. Lumsdaine, E.J. Martin, W.D. McGinnis, S.J. Meitner, L.W. Owen, H.B. Ray, V.K. Varma, The development of the material plasma exposure experiment, IEEE Trans. Plasma Sci. 44 (2016) 3456–3464, https://doi.org/10.1109/TPS.2016.2628326.

[6] J.B.O. Caughman, R.H. Goulding, T.M. Biewer, T.S. Bigelow, I.H. Campbell, J. Caneses, S.J. Diem, A. Fadnek, D.T. Fehling, R.C. Isler, E.H. Martin, C.M. Parish, J. Rapp, K. Wang, C.J. Beers, D. Donovan, N. Kafle, H.B. Ray, G.C. Shaw, M.A. Showers, Plasma source development for fusion-relevant material testing, J. Vac. Sci. Technol. Vac. Surf. Film 35 (2017) 03E114, https://doi.org/10.1116/1.4982664.

[7] J. Rapp, T.M. Biewer, T.S. Bigelow, J.F. Caneses, J.B.O. Caughman, S.J. Diem, R.H. Goulding, R.C. Isler, A. Lumsdaine, C.J. Beers, T. Bjorholm, C. Bradley, J.M. Canik, D.C. Donovan, R.C. Duckworth, R.H. Howard, N. Kafle, Y. Katoh, A. Lasa, T. Lessard, E.H. Martin, S.J. Meitner, G.-N. Luo, W.D. McGinnis, L.W. Owen, H.B. Ray, G.C. Shaw, M. Showers, V. Varma, Developing the science and technology for the Material Plasma Exposure eXperiment, Nucl. Fusion57 (2017) 116001, https://doi.org/10.1088/1741-4326/aa7b1c.

[8] C.J. Beers, R.H. Goulding, R.C. Isler, E.H. Martin, T.M. Biewer, J.F. Caneses, J.B.O. Caughman, N. Kafle, J. Rapp, Helicon plasma ion temperature measurements and observed ion cyclotron heating in proto-MPEX, Phys. Plasmas25 (2018) 013526, https://doi.org/10.1063/1.4994541.

[9] M. Showers, T.M. Biewer, J.B.O. Caughman, D.C. Donovan, R.H. Goulding, J. Rapp, Heat flux estimates of power balance on Proto-MPEX with IR imaging, Rev. Sci. Instrum. 87 (2016) 11D412, https://doi.org/10.1063/1.4959953.

[10] M. Showers, P.A. Piotrowicz, C.J. Beers, T.M. Biewer, J. Caneses, J. Canik, J.B.O. Caughman, D.C. Donovan, R.H. Goulding, A. Lumsdaine, N. Kafle, L.W. Owen, J. Rapp, H. Ray, Power accounting of plasma discharges in the linear device Proto-MPEX, Plasma Phys. Control. Fusion. 60 (2018) 065001, https://doi.org/10.1088/1361-6587/aab7c8.

[11] J. Rapp, L.W. Owen, X. Bonnin, J.F. Caneses, J.M. Canik, C. Corr, J.D. Lore, Transport simulations of linear plasma generators with the B2.5-Eirene and EMC3-Eirene codes, J. Nucl. Mater. 463 (2015) 510–514, https://doi.org/10.1016/j.jnucmat.2014.12.058.

[12] W. Fundamenski, SCRAPE-OFF LAYER TRANSPORT ON JET, Fusion Sci. Technol. 53 (2008) 1023–1063, https://doi.org/10.13182/FST08-A1746.

[13] L.W. Owen, J. Rapp, J. Canik, J.D. Lore, Transport modeling of convection dominated helicon discharges in Proto-MPEX with the B2.5-Eirene code, Phys. Plasmas24 (2017) 112504, https://doi.org/10.1063/1.5002534.

[14] R.H. Goulding, J.B.O. Caughman, J. Rapp, T.M. Biewer, T.S. Bigelow, I.H. Campbell, J.F. Caneses, D. Donovan, N. Kafle, E.H. Martin, H.B. Ray, G.C. Shaw, M.A. Showers, Progress in the development of a high power helicon plasma source for the materials plasma exposure experiment, Fusion Sci. Technol. 72 (2017) 588–594, https://doi.org/10.1080/15361055.2017.1352429org/10.1080/15361055.2017.1352429.

[15] P.A. Piotrowicz, J.F. Caneses, M.A. Showers, D.L. Green, R.H. Goulding, J.B.O. Caughman, T.M. Biewer, J. Rapp, D.N. Ruzic, Direct measurement of the transition from edge to core power coupling in a light-ion helicon source, Phys. Plasmas25 (2018) 052101, https://doi.org/10.1063/1.5023924.

[16] P.A. Piotrowicz, J.F. Caneses, D.L. Green, R.H. Goulding, C. Lau, J.B.O. Caughman, J. Rapp, D.N. Ruzic, Helicon normal modes in Proto-MPEX, Plasma Sources Sci. Technol. 27 (2018) 055016, https://doi.org/10.1088/1361-6595/aabd62.
[17] J.F. Caneses, B. Blackwell, RF compensation of double Langmuir probes: modelling and experiment, Plasma Sources Sci. Technol. 24 (2015) 35024, https://doi.org/10.1088/0963-0252/24/3/035024.
[18] B. Beal, L. Johnson, D. Brown, J. Blakely, D. Bromaghim, Improved analysis techniques for cylindrical and spherical double probes, Rev. Sci. Instrum. 83 (2012) https://doi.org/10.1063/1.4739221.
[19] T.M. Biewer, S. Meitner, J. Rapp, H. Ray, G. Shaw, First results from the Thomson scattering diagnostic on proto-MPEX, Rev. Sci. Instrum. 87 (2016) 11E518, https://doi.org/10.1063/1.4959163.
[20] F.F. Chen, Introduction to Plasma Physics and Controlled Fusion, edition 3, Springer, New York, 2015https://doi.org/10.1017/CBO9781107415324.004.
[21] J. von Seggern, J. Winter, L. Grobusch, H.G. Esser, E. Vietzke, F. Weschenfelder, C. Hollenstein, H. Künzli, G.G. Ross, M. Rubel, Properties of thin a-C/Si:H coatings applied to TEXTOR, J. Nucl. Mater. 220–222 (1995) 677–681, https://doi.org/10.1016/0022-3115(94)00564-8.
[22] V. Philipps, A. Huber, H.G. Esser, A. Pospieszczyk, B. Schweer, J. Von Seggern, W. Biel, J. Rapp, U. Samm, Impurity release and recycling behaviour in TEXTOR-94 with siliconised walls, J. Nucl. Mater. 290–293 (2001) 1190–1194, https://doi.org/10.1016/S0022-3115(00)00555-9.
[23] V. Philipps, Wall conditioning on textor, Fusion Sci. Technol. 47 (2005) 119–125 http://juser.fz-juelich.de/record/44193/files/63294.pdf.
[24] R.K. Janev, W.D. Langer, J. Post, E. Douglas, J. Evans, Kenneth, Elementary Processes in Hydrogen-helium Plasmas: Cross Sections and Reaction Rate Coefficients, Springer-Verlag, 1987https://doi.org/10.1007/978-3-642-71935-6.
[25] R. Maingi, J.G. Watkins, M.A. Mahdavi, L.W. Owen, Pump plenum pressure dependence on divertor plasma parameters and magnetic geometry in the DIII-D tokamak, Nucl. Fusion. 39 (1999) 1187–1192, https://doi.org/10.1088/0029-5515/39/9/311.
[26] W. Eckstein, Calculated Sputtering, Reflection, and Range Values: IPP 9/132, Garching http://edoc.mpg.de/283473, 2002.
[27] T. Fujimoto, K. Sawada, K. Takahata, Ratio of Balmer line intensities resulting from dissociative excitation of molecular hydrogen in an ionizing plasma, J. Appl. Phys. 66 (1989) 2315, https://doi.org/10.1063/1.344289.
[28] G.M. McCracken, M.F. Stamp, R.D. Monk, A.G. Meigs, J. Lingertat, R. Prentice, A. Starling, R.J. Smith, A. Tabasso, Evidence for volume recombination in JET detached divertor plasmas physics of ultimate detachment of a tokamak divertor plasma, Nucl. Fusion. 36 (1998) 619–629.